CCS Chemistry

RESEARCH ARTICLE

Received: Apr. 24, 2022 | Accepted: July 15, 2022 | Published: Aug. 8, 2022

Type I Photoreaction and Photoinduced Ferroptosis by a Ru(II) Complex to Overcome Tumor Hypoxia in Photodynamic Therapy

Fen Qi[1], Hao Yuan[1,2], Yuncong Chen[1,2]*, Xin-Xin Peng[1], Yanping Wu[1], Weijiang He[1]* & Zijian Guo[1,2]*

[1]*State Key Laboratory of Coordination Chemistry, School of Chemistry and Chemical Engineering, Chemistry and Biomedicine Innovation Center (ChemBIC), Nanjing University, Nanjing 210023, Jiangsu,* [2]*Nanchuang (Jiangsu) Institute of Chemistry and Health, Nanjing 210000, Jiangsu*

**Corresponding authors: chenyc@nju.edu.cn; heweij69@nju.edu.cn; zguo@nju.edu.cn*

Cite this: *CCS Chem.* **2023**, 5, 1583–1591
DOI: 10.31635/ccschem.022.202202074

Photodynamic therapy (PDT) usually shows limited efficacy in solid tumors since traditional PDT is O_2-dependent while solid tumors are inherently hypoxic. In addition, hypoxic tumor cells possess antiapoptotic pathways that resist PDT-induced apoptosis. Therefore, developing photosensitizers (PSs) that show low O_2-dependency and can induce nonapoptotic cell death pathways is critically needed. Herein, a series of Ru(II) polypyridine complex-based PSs, RuNMe, RuH, and RuCN, were synthesized, and their applications against hypoxic tumor cells through PDT were investigated. All three complexes show the ability to generate the superoxide anion radical ($\cdot O_2^-$), which is the type I photoreaction and less O_2-dependent. RuNMe shows the best PDT performance against MCF-7 cells and three-dimensional multicellular spheroids, due to its higher cellular uptake and more reactive oxygen species generation. More importantly, RuNMe-incubated MCF-7 cells show photoinduced ferroptosis as evidenced by glutathione peroxidase 4 downregulation and lipid peroxide accumulation. This work not only develops a novel ferroptosis-inducing Ru(II) complex with the type I PDT process but also offers an effective strategy to solve tumor hypoxia in PDT.

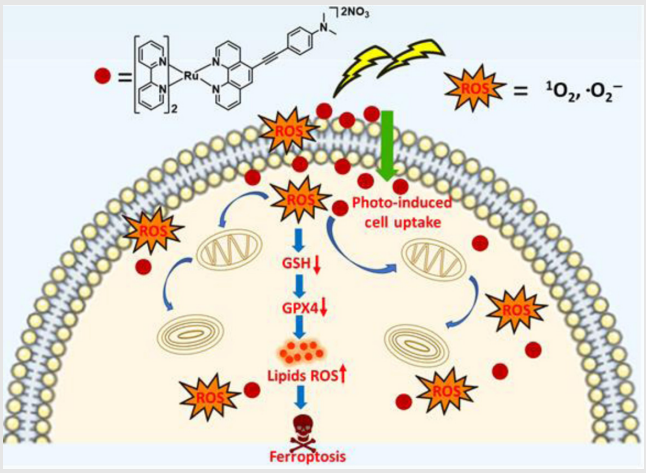

Keywords: **ferroptosis, photodynamic therapy, O_2-independent, type I photoreaction, superoxide anion radical ($\cdot O^{2-}$)**

Introduction

In the past few decades, photodynamic therapy (PDT) has become a promising method for the treatment of various diseases, especially tumors, due to its low systemic toxicity and minimal invasiveness.[1,2] Generally, photosensitizers (PSs) are injected and accumulated in tumor tissues. Light irradiation on the tumor site then produces cytotoxic reactive oxygen species (ROS), leading to suppression of the malignant tumors while

preserving the surrounding normal tissues.[3–5] PDT is mainly divided into type I (production of superoxide anion radicals, hydroxyl radicals, and hydrogen peroxide) and type II (production of $^1O_2$) photoreactions.[6–8] Most of the current reports on the PDT process are based on the type II photoreaction, which is highly dependent on the O_2 concentration.[7–9] However, hypoxia is a typical feature of the solid tumor microenvironment.[10–12] PDT-mediated O_2 consumption further exacerbates tumor hypoxia and ultimately leads to unsatisfactory therapeutic effects.[13,14] In this regard, type I PSs are more favorable since they show less O_2 dependence.[15,16] On the other hand, PDT triggers various cellular responses and induces cell death through necrosis and/or apoptosis.[17,18] However, hypoxia will induce cellular adaptations,[19] and one of these adaptations is the expression of multidrug resistance proteins (ABC transporters) that make cells resistant to apoptosis.[20] Therefore, there is an urgent need to develop PSs that show minimum O_2-dependence and induce nonapoptotic cell death pathways to improve the therapeutic effect against hypoxic tumor cells.

Ferroptosis is an iron-dependent, nonapoptotic form of cell death characterized by cytological changes, such as decreased or vanished mitochondria cristae,[21–23] and it has been recognized as a novel strategy for anticancer therapy.[24,25] ROS generated by PSs will cause rapid glutathione (GSH) consumption, resulting in suppression of glutathione peroxidase 4 (GPX4) activity and accumulation of lipid peroxides (LPOs), finally leading to ferroptosis.[26] Metal complex-based PSs have shown their potential to induce ferroptosis to effectively deplete hypoxic tumor cells. Guo et al. reported a series of Ir(III) compounds as PSs that can generate superoxide anion radicals ($\cdot O_2^-$) and hydroxyl radicals ($\cdot$OH) to overcome tumor hypoxia and induce ferroptosis in cells.[27] Ru(II) polypyridine complexes have also been widely used in PDT due to their excellent chemical and photophysical properties such as high-water solubility, high ROS generation, chemical stability, and photostability.[28–39] The ruthenium polypyridine complex TLD-1433 has entered a phase II clinical trial for the treatment of nonmuscle invasive bladder cancer.[40,41] However, most of the Ru(II) complexes cause apoptosis via photochemical processes. Ru(II)-based PSs with ferroptosis-inducing ability have not been reported.

In this study, three Ru(II) polypyridine complexes (**RuNMe**, **RuH**, and **RuCN**) were successfully synthesized as novel PSs for PDT against hypoxic tumor cells (Figure 1a). All the Ru(II) complexes showed a high quantum yield of singlet oxygen and superoxide anion radical ($\cdot O_2^-$) upon light irradiation, suggesting the coexistence of both type I and type II PDT processes. Among them, **RuNMe** showed the best tumor cell inhibition effect due to its higher cell uptake compared to that of **RuH** and **RuCN**. Upon light irradiation, MCF-7 cells cultured with

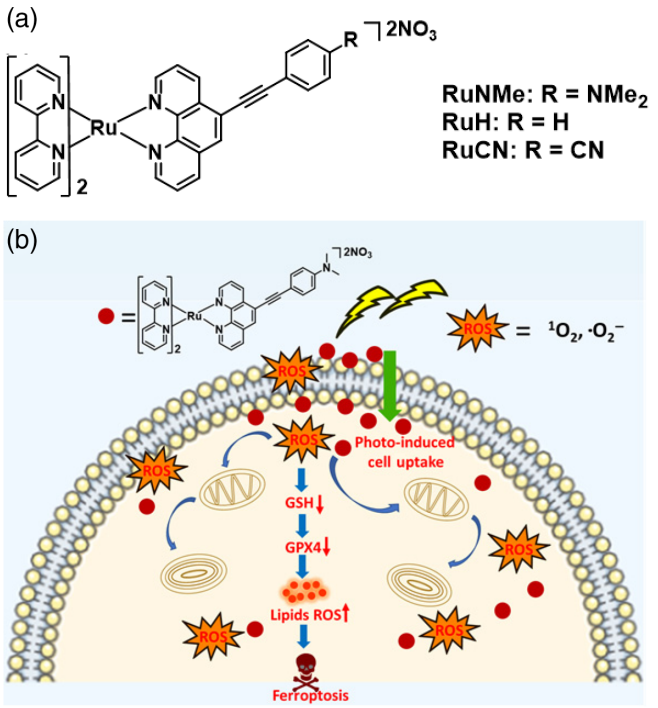

Figure 1 | *(a) Chemical structures of Ru(II) complexes. (b) The schematic illustration of the photoinduced ferroptosis mechanism by **RuNMe** upon irradiation.*

RuNMe showed distinct mitochondrial atrophy, GSH consumption, GPX4 downregulation, and LPO accumulation that can be reversed by cotreatment of ferrostatin-1 (Fer-1, a ferroptosis inhibitor), suggesting typical ferroptosis in a GPX4-dependent manner (Figure 1b). This work demonstrates that Ru(II) complex-based PSs can induce ferroptosis, providing a new and reliable method for effective PDT to overcome tumor hypoxia.

Experimental Methods

Details of the materials and instruments utilized are provided in the Supporting Information.

Preparation of Ru complexes

The synthetic routes of Ru(II) compounds are shown in Supporting Information Scheme S1. Intermediate compounds were synthesized according to the reported procedures,[28] and the Ru(II) compounds **RuNMe**, **RuH**, and **RuCN** (Figure 1a) have been successfully characterized by nuclear magnetic resonance (NMR) spectroscopy and high-resolution mass spectrometry (HRMS) (Supporting Information Figures S1–S10).

Cell culture

MCF-7 cells were cultured in RPMI-1640 media. 1640 media were supplemented with fetal bovine serum

DOI: 10.31635/ccschem.022.202202074
Citation: *CCS Chem.* **2023**, 5, 1583–1591
Link to VoR: https://doi.org/10.31635/ccschem.022.202202074

(10%, v/v), penicillin (100 units/mL), and streptomycin (50 units/mL) at 37 °C in a CO_2 incubator (5% CO_2). The experiment was divided into the following four groups:

1. Dark + Normoxia group. The cells were incubated with Ru(II) complex in the dark.
2. Dark + Hypoxia group. The cells were sealed in an anaerobic airbag for 1 h after 3 h of incubation with Ru(II) complex in the dark. Cells were taken out of the anaerobic airbag and put back in the normal incubator after 1 h. Oxygen concentration was below 0.1% during irradiation.
3. Light + Normoxia group. The cells were exposed to photoirradiation (white light 30 min) after 4 h of dark incubation with Ru(II) complex and then taken back into the incubator. Oxygen concentration was 21%.
4. Light + Hypoxia group. The cells were sealed in an anaerobic airbag 1 h before irradiation (white light 30 min) to create a hypoxic condition after 3 h of incubation with Ru(II) complex in the dark, and the irradiation was carried out in the anaerobic airbag. Cells were taken out of the anaerobic airbag and put back into a normal incubator after irradiation. Oxygen concentration was below 0.1% during irradiation.

Results and Discussion

Photophysical properties

The photophysical properties of **RuNMe**, **RuH**, and **RuCN** were investigated as shown in Supporting Information Figures S11 and S12 and Table S1. There is no significant difference in the maximum absorption wavelength with different solvents (Supporting Information Figure S11). The absorption at 400–500 nm in the visible light region is attributed to the characteristic absorption of metal-to-ligand charge transfer (MLCT) of the Ru(II) complex, which is the transition of dπ-π* (Ru(II) to *N*, *N* ligand). The broad and strong absorption at 450 nm and the shoulder peak that appeared at 420 nm can be attributed to the superposition of the absorption of the charge transfer state (MLCT) between metal Ru and different ligands, namely the dπ (Ru)-π*(bpy) (2, 2′-bipyridine) and dπ (Ru)-π* (phenanthroline ligand) superposition. The absorption band of the complex at 330 nm was the absorption peak of the *o*-phenanthroline ligand. The broad emission band centered at 602 nm was MLCT emission. As can be seen from the emission spectra of three complexes in different solvents, the fluorescence intensity increased with increasing solvent polarity (Supporting Information Figure S12). Additionally, due to the strong electron-donating properties of *N*,*N*-dimethyl, the complex **RuNMe** exhibited the photoinduced electron transfer effect, which caused its fluorescence to be significantly quenched (Supporting Information Figure S12).

The singlet oxygen ($^1O_2$) quantum yield is one of the decisive factors for the PDT effect. Consequently, the $^1O_2$ quantum yields of the Ru(II) compounds were investigated with $Ru(bpy)_3$ as the standard sample. As shown in Supporting Information Figure S13 and Table S1, compounds **RuH** and **RuNMe** had high singlet oxygen quantum yields (0.55 for **RuNMe**, 0.65 for **RuH**, and 0.32 for **RuCN**, respectively), indicating good potential for effective PDT.

Photoinduced anticancer activity of Ru(II) complexes

Then the photocytotoxicities of **RuNMe**, **RuH**, and **RuCN** against MCF-7 cells were determined (Table 1). The IC_{50} values of **RuH** determined under normoxia and hypoxia upon light irradiation were 2.3 ± 0.5 and 11.1 ± 2.3 μM while the IC_{50} values for incubation under dark conditions were 168.0 ± 5.6 and 146.2 ± 10.3 μM, respectively. The photocytotoxicity index (PI) values of **RuH** were determined to be 73 and 13 under normoxia and hypoxia by calculating the ratio of $(IC_{50})_{Dark}/(IC_{50})_{Light}$. For **RuCN**, the $(IC_{50})_{Light}$ values were 4.4 ± 0.6 and 14.9 ± 0.9 μM under normoxia and hypoxia, respectively. The PI values were 42 and 12 under normoxia and hypoxia, respectively (Table 1). The $(IC_{50})_{Light}$ values of **RuNMe** under normoxia and hypoxia (0.4 ± 0.1 and 1.5 ± 0.3 μM, respectively) were much lower than that of **RuH** and **RuCN**, concomitant with PIs of 244 and 58 under normoxia and hypoxia. The above data show that the PDT effect of **RuNMe** was much more efficient than that of **RuH** and **RuCN**. Meanwhile, the PIs of **RuNMe** under normoxia and hypoxia were about 3–5 times higher than those of **RuH** and **RuCN**.

Table 1 | *IC_{50} (μM) of Ru(II) Complexes against MCF-7 Cell Line (24 h)*

	Dark		Light	
Complexes	Normoxia	Hypoxia	Normoxia (PI)	Hypoxia (PI)
RuNMe	97.4 ± 9.6	87.7 ± 7.9	0.4 ± 0.1 (244)	1.5 ± 0.3 (58)
RuH	168.0 ± 5.6	146.2 ± 10.3	2.3 ± 0.5 (73)	11.1 ± 2.3 (13)
RuCN	185.4 ± 19.4	183.9 ± 11.7	4.4 ± 0.6 (42)	14.9 ± 0.9 (12)

Note: PI: photocytotoxicity index, the ratio of $(IC_{50})_{Dark}/(IC_{50})_{Light}$.

DOI: 10.31635/ccschem.022.202202074
Citation: *CCS Chem.* **2023**, 5, 1583–1591
Link to VoR: https://doi.org/10.31635/ccschem.022.202202074

The cellular uptake of **RuNMe**, **RuH**, and **RuCN** was determined by quantification of Ru concentration in MCF-7 cells via inductively coupled plasma mass spectrometry (ICP-MS; Supporting Information Figure S14). The results showed that the content of Ru in the cells incubated with **RuNMe** was higher than that in the cells incubated with **RuH** and **RuCN**, both under normoxia and hypoxia. Therefore, the different cytotoxicities of different complexes may be related to the different uptake of the three compounds by the cells. The octanol/water partition coefficients (logP) of **RuNMe**, **RuH**, and **RuCN** are –0.24, –1.30, and –1.50 (Supporting Information Table S1), respectively. This data demonstrate that the lipophilicity of **RuNMe** was higher than that of **RuH** and **RuCN**, resulting in higher cellular uptake. The flow cytometric annexin V-FITC assay is a typical method to monitor the destruction of cell membrane integrity.[42,43] **RuNMe**, **RuH**, and **RuCN** were incubated for 4 h in the dark, then irradiated (white light, 30 min) and further incubated for different times (1, 2, and 4 h). The FITC fluorescence of the **RuH-** and **RuCN**-incubated cells remained at a low level during the incubation while that of **RuNMe**-incubated cells increased gradually with time at a higher level (Supporting Information Figure S15). The above results indicated that the production of ROS after irradiation destroyed the cell membrane[43–45] and increased the cell uptake of **RuNMe** while the membrane of **RuH**- and **RuCN**-incubated cells had no obvious changes. This may also contribute to the differences in cellular uptake and cytotoxic activity.

Photoinduced reactive oxygen species generation in MCF-7 cells

Photoinduced intracellular ROS generation by Ru(II) complexes was investigated in MCF-7 cells. First, the $^1O_2$ generation was carefully examined with singlet oxygen sensor green (SOSG) as the probe. A significant increase in fluorescence under normoxia was observed after photoirradiation of **RuNMe**, **RuH**, and **RuCN**-incubated MCF-7 cells by confocal imaging, indicating the formation of $^1O_2$ (Figure 2a). The fluorescence inside the cell was negligible under hypoxic conditions, suggesting a typical O_2-dependent manner of $^1O_2$ generation. Then, the probe DHR123 was used to investigate the intracellular $\cdot O_2^-$ generation of the three Ru(II) complexes after irradiation. The distinct intracellular $\cdot O_2^-$ generation ability of **RuNMe** was observed, which was significantly stronger than that of **RuH** and **RuCN** under both normoxia and hypoxia (Figure 2b). A similar phenomenon was observed when DHR123 was used as a $\cdot O_2^-$ indicator in phosphate-buffered saline (PBS) buffer (Supporting Information Figure S16). The above data reveal that **RuNMe** enabled the type I photochemical process to form $\cdot O_2^-$ in MCF-7 cells under hypoxia. Consequently, **RuNMe** can function well as a PDT agent against hypoxic tumor cells.

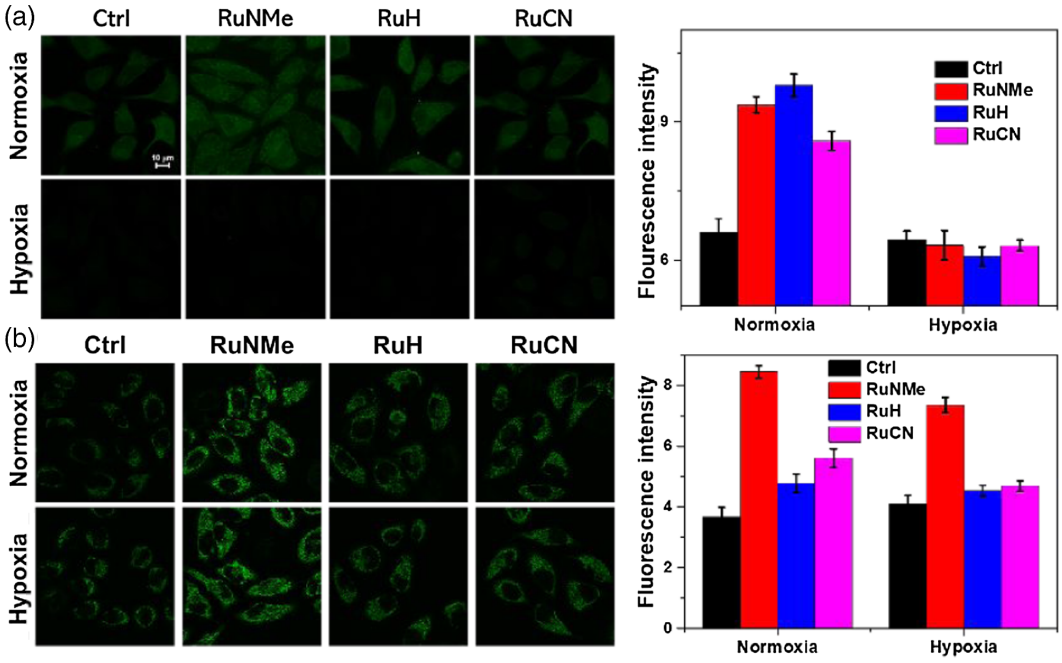

Figure 2 | *Confocal imaging of photoinduced ROS in MCF-7 cells incubated with **RuNMe**, **RuH**, and **RuCN** (3 μM, 4 h, 37 °C in the dark) under normoxia (O_2 = 21%) and hypoxia (O_2 < 0.1%) using (a) SOSG as fluorescence indicators for $^1O_2$, (b) DHR123 as fluorescence indicators for $\cdot O_2^-$. Photoirradiation was imposed with white light (8.0 J/cm^2, 30 min) after 4 h of Ru complex incubation. Scale bar: 20 μm.*

DOI: 10.31635/ccschem.022.202202074
Citation: *CCS Chem.* **2023**, 5, 1583–1591
Link to VoR: https://doi.org/10.31635/ccschem.022.202202074

Cell death mechanism study

RuNMe was chosen for the following assay since it showed the highest phototoxicity among the three complexes. The photoinduced cell death mechanism of **RuNMe**-incubated MCF-7 cells was investigated via coincubation of **RuNMe** with different cell death inhibitors (Figure 3a). The cell viabilities showed no distinct difference when MCF-7 cells were treated with inhibitors of apoptosis (*z*-VAD-*fmk*), autophagy (3-methyladenine, 3-MA), and necrosis (necrostatin-1, Nec-1), compared with the control cells without cell death inhibitor treatment. Only the ferroptosis inhibitor (Fer-1) significantly inhibited cell death, and the cell survival rate was about 88% under normoxia. A similar phenomenon was also observed under hypoxia. The ferroptosis inhibitor effectively increased the cell survival rate to 78%, suggesting that ferroptosis is the main cell death pathway by **RuNMe** in normoxia and hypoxia upon being photoinduced. The mortality of photoinduced cells is detected by coincubating MCF-7 cells with deferoxamine (DFO, an iron chelator) or holo-transferrin (an iron transporter) and **RuNMe** (Supporting Information Figure S17). The results show that the death rate of MCF-7 cells coincubated with DFO and **RuNMe** was reduced. Similar results were observed under hypoxia, indicating that ferroptosis was suppressed when intracellular iron concentration was decreased. Moreover, the photoinduced mitochondrial morphology change by **RuNMe** in MCF-7 cells was examined using transmission electron microscopy (TEM). After irradiation, the mitochondria of control cells remained almost unchanged, while the mitochondria of **RuNMe**-treated cells showed multilamellar globules, and the cristae in the inner membrane exhibited onion-like circles in both normoxia and hypoxia, indicating that mitochondria were severely damaged (Figure 3b). The structural aberrations of the mitochondria, including disrupted cristae and compromised membrane integrity, are typical hallmarks of ferroptosis.[46] The above results demonstrate that ferroptosis was the main cell death mode upon PDT treatment using **RuNMe** as the PS.

To verify the ferroptosis mechanism, other characteristics of ferroptosis were investigated (Figure 4). Tumor cells exhibited relatively high GSH levels up to 10 mM to maintain redox balance.[47–49] GSH is a cofactor of GPX4, and rapid GSH consumption can inhibit the activity of GPX4 as a cofactor.[50,51] The cell viability of MCF-7 cells with GSH and **RuNMe** coincubation was significantly increased under both normoxia and hypoxia (Figure 4a), indicating that GSH played an important role in the cell death pathway during **RuNMe**-mediated PDT. Then, the changes in intracellular GSH levels were investigated with **RuNMe**-incubate MCF-7 cells after irradiation. The GSH

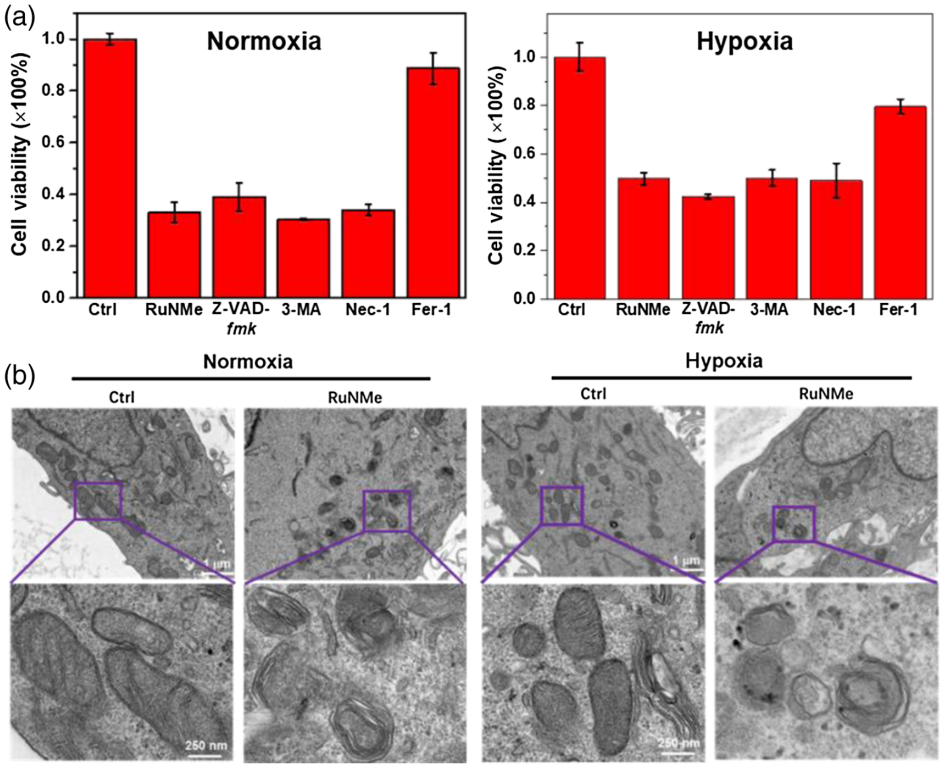

Figure 3 | *(a) Cell viabilities of MCF-7 cells upon coincubation (24 h) with **RuNMe** (3 μM) and different cell-death inhibitors:* z-*VAD-*fmk *(50 μM), 3-MA (100 μM), Fer-1 (50 μM), and Nec-1 (50 μM). (b) TEM images of the mitochondrial morphology changes in MCF-7 cells with **RuNMe** incubation upon light irradiation.*

DOI: 10.31635/ccschem.022.202202074
Citation: *CCS Chem.* **2023**, 5, 1583–1591
Link to VoR: https://doi.org/10.31635/ccschem.022.202202074

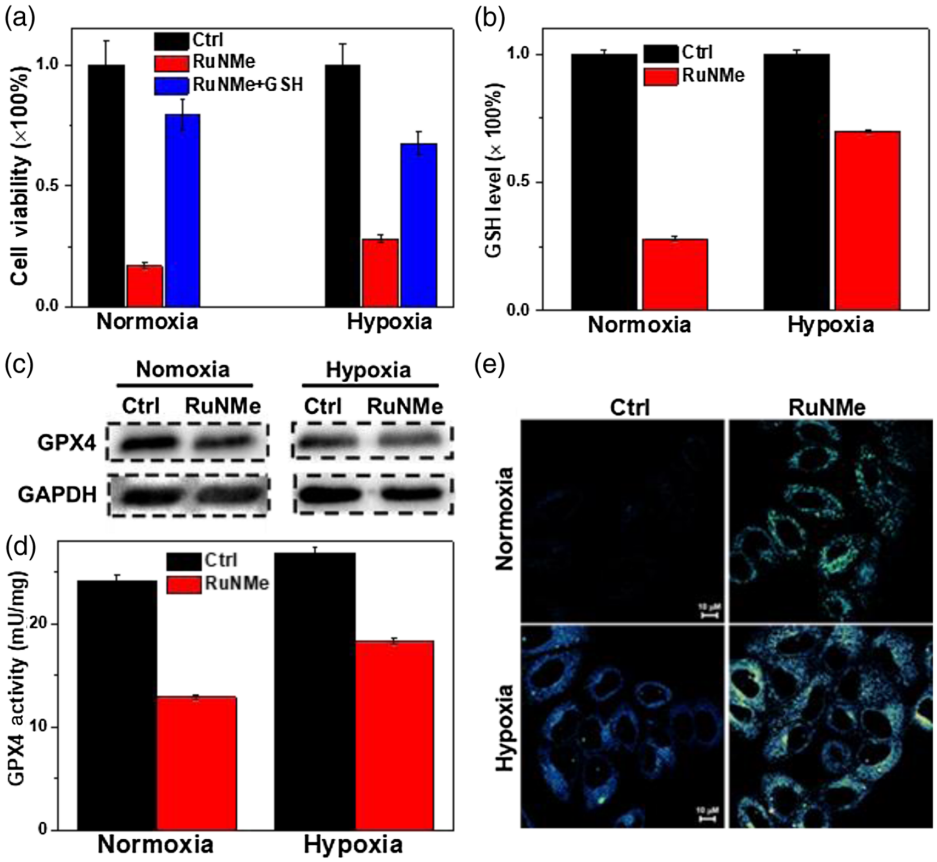

Figure 4 | *(a) The viability of MCF-7 cells treated with **RuNMe** (3 μM) and GSH (5 mM) with light irradiation. (b) GSH and oxidized glutathione disulfide (GSSG) levels in MCF-7 cells incubated with **RuNMe** (3 μM) with light irradiation. (c) Western blotting results of GPX4 expression in MCF-7 cells after treatment with **RuNMe** (3 μM). (d) The activity of GPX4 in MCF-7 cells upon incubation with **RuNMe** (3 μM) after irradiation. (e) LPOs assay of MCF-7 cells using C11-BODIPY$^{581/591}$ after coincubation with **RuNMe** (3 μM).*

level in **RuNMe**-incubated MCF-7 cells after irradiation was significantly lower than that in untreated cells under normoxia and hypoxia (Figure 4b). These results suggest that **RuNMe** efficiently reduces GSH levels and disturbs the redox balance in tumor cells.

GSH consumption of cells can inhibit the expression of GPX4 protein, thereby reducing the activity of GPX4. Upon light irradiation, distinctly decreased expression and activity of GPX4 protein in **RuNMe**-incubated MCF-7 cells were observed under both normoxia and hypoxia (Figure 4c,d). Generally, to reduce cytotoxicity, LPOs will be converted into nontoxic lipid alcohols (LOHs). However, the deactivation of GPX4 will inhibit the conversion of LPOs so the accumulation of LPOs can be regarded as an important hallmark of ferroptosis.[23,52,53] LPOs levels were monitored using the lipid peroxidation probe C11-BODIPY$^{581/591}$. Confocal imaging disclosed that **RuNMe** enhanced the probe fluorescence remarkably upon light irradiation, implying the obvious LPO accumulation under both normoxia and hypoxia (Figure 4e). These results confirm that **RuNMe** can induce ferroptosis via a GPX4-dependent pathway upon PDT.

PDT activity in three-dimensional multicellular spheroids

The above results have demonstrated that **RuNMe** can undergo the type I PDT process and induce ferroptosis, which can be very attractive as a potent PS for combating hypoxic tumor cells. Three-dimensional (3D) multicellular spheroids (MCSs) are often used to simulate the microenvironment of tumor tissues.[11,54] 3D MCSs possess a diffusion limit of approximately 150–200 μm for many molecules, which makes them an excellent model for hypoxia. Therefore, 3D MCSs with diameters of about 500 μm were used to simulate the hypoxic environment of tumor tissue (Figure 5). In the control group without Ru(II) complexes, the volume of the 3D MCSs increased distinctly after 4 days of incubation with and without irradiation. The growth of Ru(II) complexes incubated 3D MCSs was inhibited slightly under dark incubation while the growth of Ru(II) complexes treated MCSs were distinctly inhibited after irradiation. The above results show that the three Ru(II) complexes can be used as excellent type I PDT agents to overcome tumor hypoxia

DOI: 10.31635/ccschem.022.202202074
Citation: *CCS Chem.* **2023**, 5, 1583–1591
Link to VoR: https://doi.org/10.31635/ccschem.022.202202074

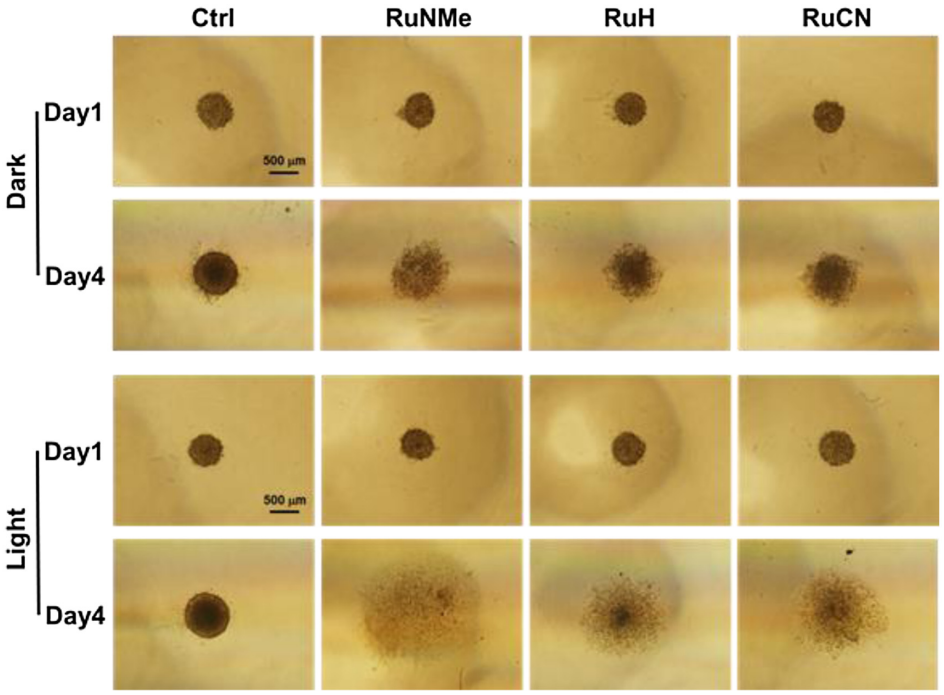

Figure 5 | *Microscopic images of MCF-7 MCSs. MCSs were incubated in the culture medium with or without 10 μM Ru complexes. Photoirradiation was imposed by white light 30 min. Scale bar: 500 μm.*

and have the potential to effectively inhibit the growth of solid tumors. Irradiation of **RuNMe**-treated 3D MCSs caused the almost complete collapse of the 3D structures of the MCSs, showing a superior PDT effect to that of **RuH** and **RuCN**.

Conclusion

Three Ru(II) complexes, **RuNMe**, **RuH**, and **RuCN**, were successfully synthesized and used as PSs to overcome tumor hypoxia during the PDT process. **RuNMe** displayed enhanced cellular uptake, higher $\cdot O_2^-$ generation and excellent PDT efficiency toward MCF-7 cells compared with **RuH** and **RuCN**. Meanwhile, **RuNMe**-incubated MCF-7 cells showed evident GPX4-dependent ferroptosis upon light irradiation under both normoxia and hypoxia. The identification of ferroptosis and its signal transduction mechanism may help to develop new therapeutic approaches that efficiently suppress the growth of hypoxic tumor cells.

Supporting Information

Supporting Information is available and includes (1) synthesis routes and methods, (2) experimental methods, (3) ^{1}H and ^{13}C NMR spectra, (4) HRMS spectra, (5) UV and FL spectra, (6) ICP-MS, (7) flow cytometric Annexin V-FITC assay, (8) photoinduced $\cdot O_2^-$ generation ability in PBS buffer, and (9) cell viability with different treatment.

Conflict of Interest

There is no conflict of interest to report.

Funding Information

This work was financially supported by the National Natural Science Foundation of China (grant nos. 22122701, 21731004, 91953201, 92153303, 21977044, and 21907050), the Natural Science Foundation of Jiangsu Province (grant nos. BK20202004 and BK20190282), and the Excellent Research Program of Nanjing University (grant no. ZYJH004).

Acknowledgments

The authors wish to acknowledge technicians Mingyi Xie, Jun Cai, Dejun Liu, and Yufei Jiang for their helpful suggestions on the experimental tests.

References

1. Castano, A. P.; Mroz, P.; Hamblin, M. R. Photodynamic Therapy and Anti-Tumour Immunity. *Nat. Rev. Cancer* **2006**, *6*, 535–545.
2. Lovel, J. F.; Tracy, W.; Liu, B.; Chen, J.; Zheng, G. Activatable Photosensitizers for Imaging and Therapy. *Chem. Rev.* **2010**, *110*, 2839–2857.

DOI: 10.31635/ccschem.022.202202074
Citation: *CCS Chem.* **2023**, 5, 1583–1591
Link to VoR: https://doi.org/10.31635/ccschem.022.202202074

3. Zhou, Z.; Ni, K.; Deng, H.; Chen, X. Dancing with Reactive Oxygen Species Generation and Elimination in Nanotheranostics for Disease Treatment. *Adv. Drug Deliv. Rev.* **2020**, *158*, 73–90.
4. Li, X.; Lovell, J. F.; Yoon, J.; Chen, X. Clinical Development and Potential of Photothermal and Photodynamic Therapies for Cancer. *Nat. Rev. Clin. Oncol.* **2020**, *17*, 657–674.
5. Zhao, X.; Liu, J.; Fan, J.; Peng, X. Recent Progress in Photosensitizers for Overcoming the Challenges of Photodynamic Therapy: From Molecular Design to Application. *Chem. Soc. Rev.* **2021**, *50*, 4185–4219.
6. Lucky, S. S.; Soo, K. C.; Zhang, Y. Nanoparticles in Photodynamic Therapy. *Chem. Rev.* **2015**, *115*, 1990–2042.
7. Fan, W.; Huang, P.; Chen, X. Overcoming the Achilles' Heel of Photodynamic Therapy. *Chem. Soc. Rev.* **2016**, *45*, 6488–6519.
8. Zhou, Z.; Song, J.; Nie, L.; Chen, X. Reactive Oxygen Species Generating Systems Meeting Challenges of Photodynamic Cancer Therapy. *Chem. Soc. Rev.* **2016**, *45*, 6597–6626.
9. Luby, B. M.; Walsh, C. D.; Zheng, G. Advanced Photosensitizer Activation Strategies for Smarter Photodynamic Therapy Beacons. *Angew. Chem. Int. Ed.* **2019**, *58*, 2558–2569.
10. Brown, J. M.; Wilson, W. R. Exploiting Tumour Hypoxia in Cancer Treatment. *Nat. Rev. Cancer* **2004**, *4*, 437–447.
11. Sharma, A.; Arambula, J. F.; Koo, S.; Kumar, R.; Singh, H.; Sessler, J. L.; Kim, J. S. Hypoxia-Targeted Drug Delivery. *Chem. Soc. Rev.* **2019**, *48*, 771–813.
12. Moulder, J. E.; Rockwell, S. Tumor Hypoxia: Its Impact on Cancer Therapy. *Cancer Metast. Rev.* **1987**, *5*, 313–334.
13. Li, X.; Jeong, K.; Lee, Y.; Guo, T.; Lee, D.; Park, J.; Kwon, N.; Na, J.-H.; Hong, S. K.; Cha, S.-S.; Huang, J.-D.; Choi, S.; Kim, S.; Yoon, J. Water-Soluble Phthalocyanines Selectively Bind to Albumin Dimers: A Green Approach Toward Enhancing Tumor-Targeted Photodynamic Therapy. *Theranostics* **2019**, *9*, 6412–6423.
14. Zhang, F. L.; Huang, Q.; Zheng, K.; Li, J.; Liu, J.-Y.; Xue, J.-P. A Novel Strategy for Targeting Photodynamic Therapy. Molecular Combo of Photodynamic Agent Zinc(II) Phthalocyanine and Small Molecule Target-Based Anticancer Drug Erlotinib. *Chem. Commun.* **2013**, *49*, 9570–9572.
15. Zhao, Y. Y.; Zhang, L.; Chen, Z.; Zheng, B.-Y.; Ke, M.; Li, X.; Huang, J. D. Nanostructured Phthalocyanine Assemblies with Efficient Synergistic Effect of Type I Photoreaction and Photothermal Action to Overcome Tumor Hypoxia in Photodynamic Therapy. *J. Am. Chem. Soc.* **2021**, *143*, 13980–13989.
16. Li, X.; Lee, D.; Huang, J. D.; Yoon, J. Phthalocyanine-Assembled Nanodotsas Photosensitizersfor Highly Efficient Type I Photoreactionsin Photodynamic Therapy. *Angew. Chem. Int. Ed.* **2018**, *57*, 9885–9890.
17. Yin, H.; Ye, X.; Niu, Q.; Wang, C.; Li, Y. Time Course of Apoptosis Induced by Photodynamic Therapy with PsD007 in LT12 Acute Myeloid Leukemia Cells. *Lasers Med. Sci.* **2016**, *31*, 817–824.
18. Song, L.; Li, C.; Zhou, Y.; Dai, F.; Luo, X.; Wang, B.; Ni, J.; Liu, Q. O_2 and Ca^{2+} Fluxes as Indicators of Apoptosis Induced by Rose Bengal–Mediated Photodynamic Therapy in Human Oral Squamous Carcinoma Cells. *Photomed. Laser Surg.* **2015**, *33*, 258–265.
19. Liu, J.; Chen, C.; Wei, T.; Gayet, O.; Loncle, C.; Borge, L.; Dusetti, N.; Ma, X.; Marson, D.; Laurini, E.; Pricl, S.; Gu, Z.; Iovanna, J.; Peng, L.; Liang, X.-J. Dendrimeric Nanosystem Consistently Circumvents Heterogeneous Drug Response and Resistance in Pancreatic Cancer. *Exploration* **2021**, *1*, 21–34.
20. Flamant, L.; Notte, A.; Ninane, N.; Raes, M.; Michiels, C. Anti-Apoptotic Role of HIF-1 and AP-1 in Paclitaxel Exposed Breast Cancer Cells under Hypoxia. *Mol. Cancer* **2010**, *9*, 191.
21. Angeli, J. P. F.; Shah, R.; Pratt, D. A.; Conrad, M. Ferroptosis Inhibition: Mechanisms and Opportunities. *Trends Pharmacol. Sci.* **2017**, *38*, 489–498.
22. Ueda, S.; Nakamura, H.; Masutani, H.; Sasada, T.; Yonehara, S.; Takabayashi, A.; Yamaoka, Y.; Yodoi, J. Redox Regulation of Caspase-3(-like) Protease Activity: Regulatory Roles of Thioredoxin and Cytochrome c. *J. Immunol.* **1999**, *161*, 6689–6695.
23. Liu, M.; Liu, B.; Liu, Q.; Du, K.; Wang, Z.; He, N. Nanomaterial-Induced Ferroptosis for Cancer Specific Therapy. *Coord. Chem. Rev.* **2019**, *382*, 160–180.
24. Wen, Y.; Chen, H.; Zhang, L.; Wu, M.; Zhang, F.; Yang, D.; Shen, J.; Chen, J. Glycyrrhetinic Acid Induces Oxidative/Nitrative Stress and Drives Ferroptosis through Activating NADPH Oxidases and iNOS, and Depriving Glutathione in Triple-Negative Breast Cancer Cells. *Free Radic Biol. Med.* **2021**, *173*, 41–51.
25. Han, J.; Kang, H.; Li, X.; Kwon, N.; Li, H.; Park, S.; Yoon, J. Photo-Fenozyme Nanoparticles Based on Fe(II)-Coordination-Driven Cyanine-Based Amino Acid Assembly for Photodynamic Ferrotherapy. *ACS Appl. Nano Mater.* **2021**, *4*, 5954–5962.
26. Yang, W. S.; Stockwell, B. R. Ferroptosis: Death by Lipid Peroxidation. *Trends Cell Biol.* **2016**, *26*, 165–176.
27. Yuan, H.; Han, Z.; Chen, Y.; Qi, F.; Fang, H.; Guo, Z.; Zhang, S.; He, W. Ferroptosis Photoinduced by NewCyclometalated Iridium(III Complexes and Its Synergism with Apoptosis in Tumor Cell Inhibition. *Angew. Chem. Int. Ed.* **2021**, *60*, 8174–8181.
28. Lincoln, R.; Kohler, L.; Monro, S.; Yin, H.; Stephenson, M.; Zong, R.; Chouai, A.; Dorsey, C.; Hennigar, R.; Thummel, R. P.; McFarland, S. A. Exploitation of Long-Lived 3IL Excited States for Metal-Organic Photodynamic Therapy: Verification in a Metastatic Melanoma Model. *J. Am. Chem. Soc.* **2013**, *135*, 17161–17175.
29. Wei, F.; Kuang, S.; Rees, T. W.; Liao, X.; Liu, J.; Luo, D.; Wang, J.; Zhang, X.; Ji, L.; Chao, H. Ruthenium(II) Complexes Coordinated to Graphitic Carbon Nitride: Oxygen Self-Sufficient Photosensitizers which Produce Multiple ROS for Photodynamic Therapy in Hypoxia. *Biomaterials* **2021**, *276*, 121064.
30. Huang, H.; Banerjee, S.; Qiu, K.; Zhang, P.; Blacque, O.; Malcomson, T.; Paterson, M. J.; Clarkson, G. J.; Staniforth, M.; Stavros, V. G.; Gasser, G.; Chao, H.; Sadler, P. J. Targeted Photoredox Catalysis in Cancer Cells. *Nat. Chem.* **2019**, *11*, 1041–1048.

DOI: 10.31635/ccschem.022.202202074
Citation: *CCS Chem.* **2023**, 5, 1583–1591
Link to VoR: https://doi.org/10.31635/ccschem.022.202202074

31. Xiong, T.; Li, M.; Chen, Y.; Du, J.; Fan, J.; Peng, X. A Singlet Oxygen Self-Reporting Photosensitizer for Cancer Phototherapy. *Chem. Sci.* **2020**, *12*, 2515–2520.
32. Li, M.; Shao, Y.; Kim, J. H.; Pu, Z.; Zhao, X.; Huang, H.; Xiong, T.; Kang, Y.; Li, G.; Shao, K.; Fan, J.; Foley, J. W.; Kim, J. S.; Peng, X. Unimolecular Photodynamic O_2-Economizer to Overcome Hypoxia Resistance in Phototherapeutics. *J. Am. Chem. Soc.* **2020**, *142*, 5380–5388.
33. Wu, Y.; Li, S.; Chen, Y.; He, W.; Guo, Z. Recent Advances in Noble Metal Complex Based Photodynamic Therapy. *Chem. Sci.* **2022**, *13*, 5085–5106.
34. Notaro, A.; Jakubaszek, M.; Rotthowe, N.; Maschietto, F.; Vinck, R.; Felder, P. S.; Goud, B.; Tharaud, M.; Ciofini, I.; Bedioui, F.; Winter, R. F.; Gasser, G. Increasing the Cytotoxicity of Ru(II) Polypyridyl Complexes by Tuning the Electronic Structure of Dioxo Ligands. *J. Am. Chem. Soc.* **2020**, *142*, 6066–6084.
35. Karges, J.; Kuang, S.; Maschietto, F.; Blacque, O.; Ciofini, I.; Chao, H.; Gasser, G. Rationally Designed Ruthenium Complexes for 1- and 2-Photon Photodynamic Therapy. *Nat. Commun.* **2020**, *11*, 3262.
36. Wachter, E.; Moya, D.; Glazer, E. C. Combining a Ru(II) "Building Block" and Rapid Screening Approach to Identify DNA Structure-Selective "Light Switch" Compounds. *ACS Comb. Sci.* **2017**, *19*, 85–95.
37. Chakrabortty, S.; Agrawalla, B. K.; Stumper, A.; Vegi, N. M.; Fischer, S.; Reichardt, C.; Kögler, M.; Dietzek, B.; Feuring-Buske, M.; Buske, C.; Rau, S.; Weil, T. Mitochondria Targeted Protein-Ruthenium Photosensitizer for Efficient Photodynamic Applications. *J. Am. Chem. Soc.* **2017**, *139*, 2512–2519.
38. Swaminathan, S.; Haribabu, J.; Balakrishnan, N.; Vasanthakumar, P.; Karvembu, R. Piano Stool Ru(II)-arene Complexes Having Three Monodentate Legs: A Comprehensive Review on Their Development as Anticancer Therapeutics Over the Past Decade. *Coord. Chem. Rev.* **2022**, *459*, 214403.
39. Han, Z.; Chen, Y.; Wang, Y.; Shi, X.; Yuan, H.; Bai, Y.; Chen, Z.; Fang, H.; He, W.; Guo, Z. Photoinduced Synergistic Cytotoxicity Towards Cancer Cells via Ru(II) Complexes. *Dalton Trans.* **2020**, *49*, 13954–13957.
40. Monro, S.; Colon, K. L.; Yin, H., Roque, III, J.; Konda, P.; Gujar, S.; Thummel, R. P.; Lilge, L.; Cameron, C. G.; McFarland, S. A. Transition Metal Complexes and Photodynamic Therapy from a Tumor-Centered Approach: Challenges, Opportunities, and Highlights from the Development of TLD1433. *Chem. Rev.* **2019**, *119*, 797–828.
41. McFarland, S. A.; Mandel, A.; Dumoulin-White, R.; Gasser, G. Metal-Based Photosensitizers for Photodynamic Therapy: The Future of Multimodal Oncology? *Curr. Opin. Chem. Biol.* **2020**, *56*, 23–27.
42. Okada, H.; Mak, T. W.; Okada, H.; Mak, T. W. Pathways of Apoptotic and Non-Apoptotic Death in Tumour Cells. *Nat. Rev. Cancer* **2004**, *4*, 592–603.
43. Xue, X.; Zhu, C.; Chen, H.; Bai, Y.; Shi, X.; Jiao, Y.; Chen, Z.; Miao, Y.; He, W.; Guo, Z. A New Approach to Sensitize Antitumor Monofunctional Platinum(II) Complexes via Short Time Photo-Irradiation. *Inorg. Chem.* **2017**, *56*, 3754–3762.
44. Xue, X.; Qian, C.; Fang, H.; Liu, H.-K.; Yuan, H.; Guo, Z.; Bai, Y.; He, W. Photoactivated Lysosomal Escape of a Monofunctional PtII Complex Pt-BDPA for Nucleus Access. *Angew. Chem. Int. Ed.* **2019**, *58*, 12661–12666.
45. Wang, B.; Yuan, H.; Liu, Z.; Nie, C.; Liu, L.; Lv, F.; Wang, Y.; Wang, S. Cationic Oligo(p-Phenylene Vinylene) Materials for Combating Drug Resistance of Cancer Cells by Light Manipulation. *Adv. Mater.* **2014**, *26*, 5986–5990.
46. Galluzzi, L.; Vitale, I. Molecular Mechanisms of Cell Death: Recommendations of the Nomenclature Committee on Cell Death 2018. *Cell Death Differ.* **2018**, *25*, 486–541.
47. He, H.; Du, L.; Guo, H.; An, Y.; Lu, L.; Chen, Y.; Wang, Y.; Zhong, H.; Shen, J.; Wu, J.; Shuai, X. Redox Responsive Metal Organic Framework Nanoparticles Induces Ferroptosis for Cancer Therapy. *Small* **2020**, *16*, e2001251.
48. Ling, X.; Chen, X.; Riddell, I. A.; Tao, W.; Wang, J.; Hollett, G.; Lippard, S. J.; Farokhzad, O. C.; Shi, J.; Wu, J. Glutathione-Scavenging Poly(disulfide amide) Nanoparticles for the Effective Delivery of Pt(IV) Prodrugs and Reversal of Cisplatin Resistance. *Nano Lett.* **2018**, *18*, 4618–4625.
49. Meng, X.; Deng, J.; Liu, F.; Guo, T.; Liu, M.; Dai, P.; Fan, A.; Wang, Z.; Zhao, Y. Triggered All-Active Metal Organic Framework: Ferroptosis Machinery Contributes to the Apoptotic Photodynamic Antitumor Therapy. *Nano Lett.* **2019**, *19*, 7866–7876.
50. Angeli, J. P. F.; Schick, J. A.; Conrad, M. Inactivation of the Ferroptosis Regulator Gpx4 Triggers Acute Renal Failure in Mice. *Nat. Cell Biol.* **2014**, *16*, 1180–1191.
51. Yang, W.; Sriramaratnam, R.; Welsch, M.; Shimada, K.; Skouta, R.; Viswanathan, V. S.; Cheah, J. H.; Clemons, P. A.; Shamji, A. F.; Clish, C. B.; Brown, L. M.; Girotti, A. W.; Cornish, V. W.; Schreiber, S. L.; Stockwell, B. R. Regulation of Ferroptotic Cancer Cell Death by GPX4. *Cell* **2014**, *156*, 317–331.
52. Gao, M. H.; Yi, J. Role of Mitochondria in Ferroptosis. *Mol. Cell* **2018**, *73*, 354–363.
53. Seibt, T. M.; Proneth, B.; Conrad, M. Role of GPX4 in Ferroptosis and Its Pharmacological Implication. *Free Radical Biol. Med.* **2019**, *133*, 144–152.
54. Sun, L.; Chen, Y.; Kuang, S.; Li, G.; Guan, R.; Liu, J.; Ji, L.; Chao, H. Iridium(III) Anthraquinone Complexes as Two-Photon Phosphorescence Probes for Mitochondria Imaging and Tracking under Hypoxia. Chem. Eur. J. **2016**, 22, 8955–8965.

DOI: 10.31635/ccschem.022.202202074
Citation: *CCS Chem.* **2023**, 5, 1583–1591
Link to VoR: https://doi.org/10.31635/ccschem.022.202202074